E|DPC-2015

Electric Drives Production Conference 2015

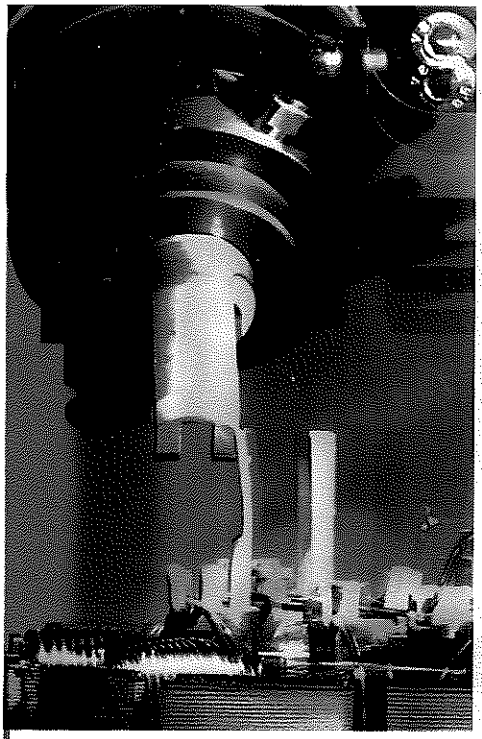

2015 5th International Conference

Electric Drives Production

September 15th – 16th, 2015
Nuremberg, Germany

Proceedings

MARSILLI

AMA Verband für Sensorik und Messtechnik e.V. – Linking Innovators

antriebstechnik

Automation Valley Nord-Bayern

Bayern Innovativ

cluster mechatronik & automation

ECPE

EEM

ETG Power Engineering Society within VDE

VDE

FVA

ZVEI

IHK Industrie- und Handelskammer Nürnberg für Mittelfranken

MH

metropolregion nürnberg

UK Magnetic Society

pels IEEE Power Electronics Society

IEEE

VDMA Antriebstechnik

mesago Messe Frankfurt Group

E|Drive-Center Bayerisches Technologiezentrum für elektrische Antriebstechnik

Compact machine design of an integrated multiphase VPMSM

T. Grosse, D. Franck, N. Conzelmann and Kay Hameyer
Institute of Electrical Machines, RWTH Aachen University
Aachen, Germany
e-mail: thorben.grosse@iem.rwth-aachen.de

D. Paul, C. Haenelt and A. Stapelmann
ThyssenKrupp Presta Camshafts
Chemnitz, Germany
e-mail: daniel.paul@thyssenkrupp.com

***Abstract* — Due to the effort designing high efficient electric vehicles, high speed traction drives are frequently used. Nowadays different winding topologies, rotor shapes and cooling concepts are studied to enlarge efficiency and power density. The application of a compact multi-phase winding permanent magnet excited synchronous machine including an active rotor cooling system provides opportunities to meet the high requirements of a traction drive. This contribution focuses on the construction and characteristics of the engineered six-phase motor and the potential to increase the machine's performance by the integrated rotor cooling system.**

Keywords* — *Electrical machines, multi phase winding systems, efficient cooling techniques

I. Motivation

Rotational speeds beyond 10,000 rpm and high power densities, both characteristics of a PMSM, provide high efficient traction drives [1]. In order to meet the stringent requirements on the traction drive of an electric vehicle, a permanent magnet excited synchronous machines with V-shaped buried magnets (VPMSM) and distributed windings is applied. To reduce the losses with increasing power density a multi-phase winding is evaluated. Furthermore, the integrated innovative rotor cooling provides the potential to enhance efficiency by lowering the temperature in the machine core.

II. Problem Statement

Multi-phase winding systems provide the possibility to avoid a large part of harmonics and therefore improve the machine's characteristics [2]. In addition to the enhancement of performance the influence on the installation space has to be studied. In contrast to a conventional star-connected three-phase motor each phase of the six-phase machine will be driven independently - hence, the machine has 12 joints instead of three. The implementation of a rotor cooling system requires a sophisticated motor design in order to achieve an optimized cooling media flow without foiling the machine's overall efficiency. Thus, the constraint of a large borehole diameter of the rotors lamination is defined to allow light weight optimization and even more important to create sufficient inner space for implementation of the cooling system ensuring an adequate air flow. As a consequence, the inner radius of the bearing has to increase considerably on the non drive end, which leads to a technical conflict at speeds of 10,000 rpm because of the enormous centrifugal forces. The dimensioning of rotor and the bearing has an immediate influence on the geometry of the housing and the machine's stator. Based on the demand to provide a very compact machine, there are high requirements on the machine design meeting the boundary conditions.

III. Design and Cooling Concept

The main objective is the application of a high dynamic and efficient six-phase traction drive with an integrated active rotor cooling system while meeting the stringent geometric constraints. Hence, the outer radius of the active components (rotor, stator) is limited to 100 mm and the entire length of the motor is restricted to 200 mm. The machine has to meet a continuous output power rating of 30 kW with a maximal torque of 150 Nm and a maximal speed of 10,000 rpm.

A. Design of the machine

Apart from the electromagnetic design of the six-phase motor this contribution focuses on the technical integration and matching of active components, housing and rotor cooling system, as this is not state of the art. In Figure 1 the entire drive-unit is shown in longitudinal section.

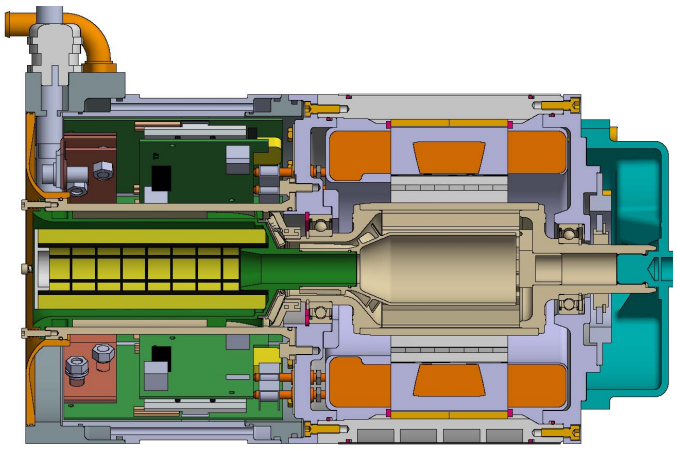

Fig. 1. Longitudinal section of the entire drive-unit.

978-1-4673-7512-2/15/$31.00 ©2015 IEEE

The drive-unit consists of two main parts: The inverter, including the feedthrough of the rotor cooling, and the electrical traction drive with its active part of the cooling system. To improve the handling and the EMC (electromagnetic compatibility) characteristics the electric connection of these two parts is realized as a plug-in connection. The supply air of the rotor cooling is absorbed through a filter on the left-hand side, passes through the inverter and motor, gets diverted in the hollow shaft and leaves the system via diffusor by the inverter. The bearing at the non drive end and the active part of the rotor have a large inner diameter to expand the installation space of the cooling system enabling a maximized air flow. The distributed windings occupy a substantial proportion of the installation space. In order to increase the compactness, the housing is adapted exactly to the geometry of the end windings and the resolver is integrated into the gearbox.

1) Active Components

Figure 2 shows the cross section of the active parts of the studied motor topology including the hollow shaft of the rotor.

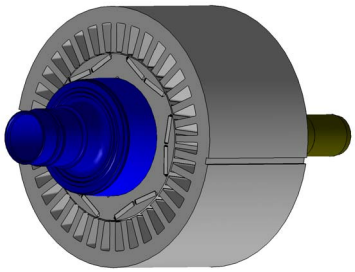

Fig. 2. Active components of the motor including the hollow shaft.

The rotor exhibits a large inner radius, in order to permit the integration of the rotor cooling - hence, the resulting rotor core is designed as a ring, according to Figure 3.b. The magnets have to be placed in a way that neither the mechanical tensile yield limit of the material is exceeded nor the saturation effects become too pronounced. Necessarily, the outer diameter of the rotor increases which results in a reduced copper cross section in the stator slots and a slim stator yoke. This causes local saturation effects during the operation and reduces the installation space for the end windings on the front end of the stator. Thus, the axial height of the end windings rises. The final cross sections of rotor and stator are shown in Figure 3.

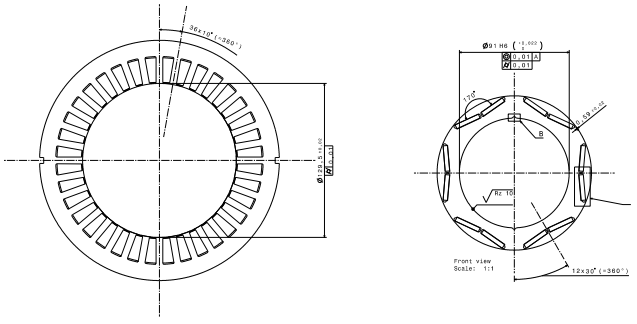

(a) Cross section of stator. **(b)** Cross section of rotor.

Fig. 3. Cross-section of the studied six-phase motor.

Figure 1 shows that the tapering of the stator yoke provokes the axial height of the windings ends so far that it ceases immediately in front of the bearing cap. A further rise of the windings is not possible since there need to remain space for the vacuum encapsulation.

2) Winding Design

The VPMSM is constructed with m = 6 phases, N = 36 slots and 2p = 6 poles. The number of slots per pole and phase q is calculated according to (1).

$$q = \frac{N}{2\,p\,m} \tag{1}$$

This results in q = 1 for the machine. The supply voltage U_{Bat} is set to 100 V in this study. Since the motor's supply voltage influences the winding construction, the low voltage, as it is chosen in this study, causes high electrical currents and consequently leads to large conductor cross sectional areas and a low number of windings.

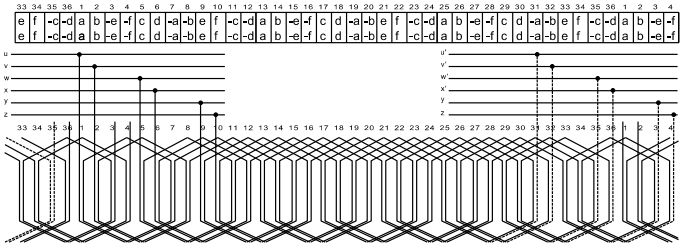

Fig. 4. Winding scheme of the six-phase motor.

The winding scheme of the six-phase winding is depicted in Figure 4. The number of windings per slot is set to eight. Since the number of slots per pole and phase is q = 1 the windings are not grouped. Although, shortening the coil pitch of the coil span by one slot provides a reduction of the harmonic content it is not implemented. In contrast to a conventional three-phase machine with the same number of slots and poles the amplitudes of the 5th and 7th harmonic are reduced by the six-phase winding system sufficiently. According to (2) shortening the coil pitch by one slot would have an insufficient effect on the lower harmonics but decreases the fundamental wave.

$$\xi_\nu = \xi_{d,\nu} \cdot \xi_{p,\nu} = \frac{\sin\left(\frac{\nu\,\pi}{2\,m}\right)}{q\,\sin\left(\frac{\nu\,\pi}{2\,m\,q}\right)} \cdot \sin\left(\nu\,\frac{\pi}{2}\,\frac{W}{\tau_p}\right) \tag{2}$$

Where the natural number ν is the ordinal number of the odd harmonics and $\frac{W}{\tau_P}$ represents the shortened coil pitch of the coil span. Shortening the coil pitch of the coil span by two slots the pitch factor of the fundamental wave gets reduced to 0.866. The pitch factor of the 11th and 13th harmonic also represents 0.866 according to (2). Therefore, there is no need shortening the coil pitch since the reduction of the fundamental wave is too pronounced and the winding ends would be too high. The more coil sections there are in the machine, the more intersection are on the winding end. Corresponding to Figure 1 and the results in the previous chapter there is no additional

installation space available, which prohibits the expansion of the end windings.

The winding factor of the fundamental wave ξ_1 which is the result of the product of the distribution factor $\xi_{d,1}$ and the shortening pitch factor $\xi_{p,1}$ can be calculated according to (2). Since the studied machine is constructed for a winding with $q = 1$ and $\frac{W}{\tau_P} = 1$ the resulting winding factor ξ_1 of the fundamental wave also equals to 1. In order to eliminate the main part of the cogging torque the stator is skewed by one tooth pitch. Consequently, the six-phase winding system enables a winding configuration that eliminates a major part of the parasitic harmonics and maximizes the machine's utilization.

3) Rotor composition and assembly

To reduce rotating masses and remove inactive rotor lamination material, there is a rotor shaft built based on a simple tube as center part. The multi part architecture as shown in Figure 5 enables the combination of different materials for each part of the shaft appropriate to its function, the ease of scalability via tube length, low component costs and flexibility. The shafts large outer diameter of 91 mm allows reducing pressure in the interference fit of the rotor lamination thus lowers material stress and supports its undisturbed electromagnetic performance. Compared to a state of the art massive rotor shaft with a diameter 55 mm, the tensile stress on the lamination inner bore is 39 % lower.

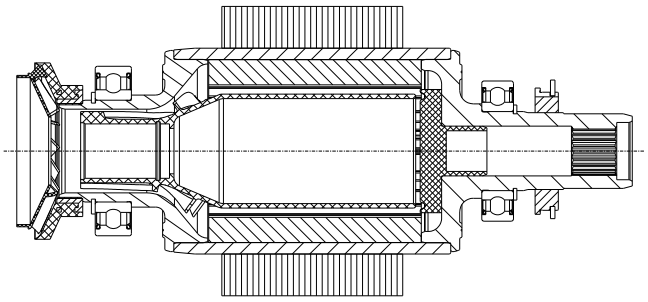

Fig. 5. Rotor shaft with lamination fit.

Inside the rotors shaft there is a space of more than 0.6 l. Due to high power density requirements there are only few and small areas available for transferring heat caused by machine losses in the rotor. A rarely used opportunity is adding an internal rotor cooling to the state of the art water cooling of the stators housing. The specific rotor design enables implementing additional components into hollow space within the shaft while assembly. This increases surface area for heat transfer by 66 % up to 0.07 m² and moreover creates turbulence of the volumetric flow. Choice of cooling media is influenced by geometric constraints and overall drive train layout. (For different machine types both gas and liquid have been developed and tested.)

Advantageous especially for high speed motors, the shaft integrated gas cooling causes the machine to be encapsulated and hence protected against abrasion debris by bearings on either side.

4) Systempackaging

The six-phase machine, has a compact design and provides a power density of about 3000 kW/m^3 and an efficiency of up to 97.0 %. The motor is designed as a separate module and can be attached to the inverter by using a plug-in connection. In Figure 6 the mounted stator and rotor are pictured. The twelve jacks and the interface of the hollow shaft of the rotor cooling system can be identified in Figure 6.(a) on the front side of the housing. In Figure 6.(b) the assembled rotor shaft is depicted. As can be seen in longitudinal section in Figure 1, the diameter of the shaft on the operation side is large to ensure maximum cross section for the pipes of the gas cooling flow.

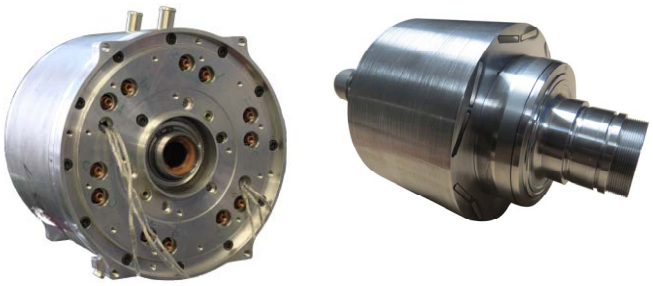

(a) Housing of the studied motor. **(b)** Rotor of the studied motor.

Fig. 6. The studied six-phase motor.

After joining the stator into the housing, it gets vacuum encapsulated to improve the machines thermal characteristics [3]. In order to maximize the thermal dissipation the cooling section of the stator is extended axially including the end windings, connecting them to the cooling section. To comply with the geometric restrictions (regarding the encapsulated construction space) and to position the sockets in their exact final position a casting device is constructed and used to form the encapsulation.

In the winding process the end windings on the non drive end are bent radial inwards over the space of the active part of the rotor (Figure 1) in order to meet the axial length limitation, set by the jacks. The end windings on the non drive end show such an axial height, that the 2-3 mm thin encapsulating layer above the winding ends moulds the jacks. Thus, they cannot be repositioned without damaging encapsulation after casting process.

Adjusting the winding ends affects two facts: The casting device has to be adapted and mounting the rotor can only be done from the drive end in packaging. During the packaging all active and housing components are assembled. The complex structure of the six-phase motor and the enormous lack of space require a sophisticated procedure to enable packaging all parts without damaging any component. At this point, all the parts to be assembled are positioned on a mounting spindle and are merged sequentially. This is only possible since the bearing shoulder on the operating side is constructed, that it fits through the tapering of the end windings.

The bearing shield at the non drive end is already positioned, the spindle penetrates the end plate and the stator fixing the remaining components at the drive side. When moving the components into each other the exact position of

the motor and the precise aligned shaft prevent a contact between stator and rotor, which would result in a damage to the motor. The sophisticated reconciliation of the system allows an accurate and precise positioning of all parts. After joining the components, the sockets are insulated embedded into the bearing shield. By accurate positioning of the jacks during encapsulation using the positioning unit of the casting device, it is ensured that all 12 jacks fit exactly through the corresponding cut-outs in the bearing shield, according to Figure 5.(a).

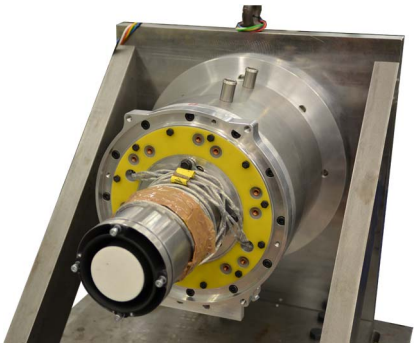

Fig. 7. Complete mounted drive-unit: Consisting of motor and gas cooling.

In Figure 7, the engine including the gas cooling and the electrical jacks is illustrated. The jacks have a cross section of 26.42 mm^2 and therefore can drive the rated continuous current of 110 A.

B. *Cooling concept*

Gas cooling

Using gas in an open circuit saves space and cost for heat exchange but, when taking air from ambient atmosphere, requires filtration. As a result of traction drive train layout often the gear side of the shaft is closed by toothing, therefore both inlet and outlet of gas are required to be spaced inside shaft opening on the inverter end of the rotor. Restriction is to only insignificantly increase that cross section and thus bearing diameter because of bearing friction issue.

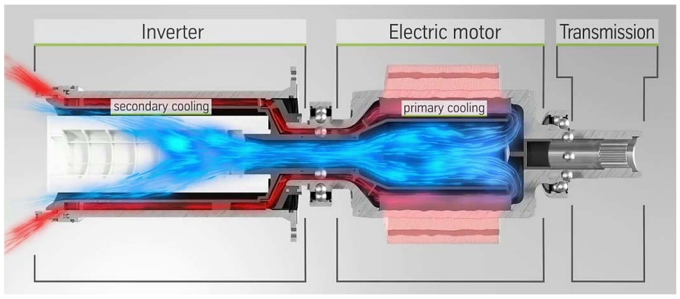

Fig. 8. General layout of multi part rotor shaft with internal cooling

The six-phase inverter is designed as hollow cylinder leaving a diameter 80 mm hole for gas flow and implementation of filtration device. Flow cross sections are calculated and parted such as both directions equal. Compared to liquids, gas has a much lower thermal capacity, $c_{air} = 1.005$ kJ/kgK vs. $c_{water} = 4.182$ kJ/kgK. For heat transmission with gas high volumetric flows are inevitable. A rotor attached fan designed as diagonal built creates up to 9.5 l/s air flow at 10,000 rpm, but already at lower speeds there are reasonable flow rates, Figure 9. Between simulation and measured volumetric flow there is a difference, caused by length and cross section of the measuring devices which are added to the assembly for recording data.

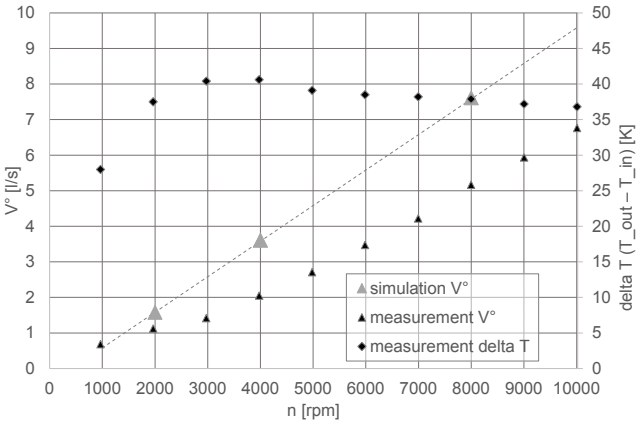

Fig. 9. Temperature and flow rate data as measured on test bench at 100°C rotor temperature

Gas cooling performance

An extrusion molded, ribbed aluminum cooler is placed inside hollow middle section of the rotor shaft's tube during assembly. An axial slot enables pre loaded assembly and therewith full contact between tube and cooler throughout operating temperature despite different coefficient of thermal expansion of materials. A crucial aspect with an innovative solution is the requirement of a static, non-rotating body within rotor shaft. It firstly separates fresh inlet gas from warmed up outlet gas and secondly carries guiding structures to untwist the gas flow when released from cooler ribs in order to create a mere axial flow. Thus it enables the fans function which is unable to work on an already twisted gas input. A dip tube when mounting motor to inverter realizes static fixation of the non-rotating body.

On a specific test bench, equipped with sensor technology, rotor temperature can be adjusted freely by induced energy thus enabling for wide range of testing. High differences between inlet and outlet air temperature document and quantize heat transfer, e.g. delta of more than 35 K at rotor temperature 100 °C during a wide speed range as shown in Figure 9. Heat quantity calculations show a dissipation of up to 300 W at maximum speed. Proportionality of flow rate and hence heat transfer with rotational speed of rotor match up well with the frequency based machine losses increase. As shown in Figure 9 speed related gas cooling capability implements a significant advantage. Validation shows ambient air in a specifically layouted cooling track being a considerable means for heat dissipation in addition to stator cooling, Figure 8. Heat transmitted by inverter in a secondary cooling area is not yet been included in testing and calculated heat dissipation. Concluding, an operational test of the overall set-up with inverter and gear proofed functionality of efficient cooling with air.

IV. Modeling of a six-phase PMSM

In further investigations the presented machine will be tested on a test bench. To operate and control the PMSM a suited machine model has to be developed considering the six-phase winding.

The inductances are one of the main parameters modeling an electric machine and are computed by FEM (finite elemente) simulation to allow a detailed study of the machine's characteristics. Due to the six-phase winding the machine inductances are represented by a six by six inductance matrix consisting of six self-inductances and 30 mutual inductances. Since the magnets are V-shaped buried in the rotor the inductances show a distinct rotor position dependency caused by its saliency ratio [6]. A typical self-inductance is shown in Figure 1, where γ is the rotor angle.

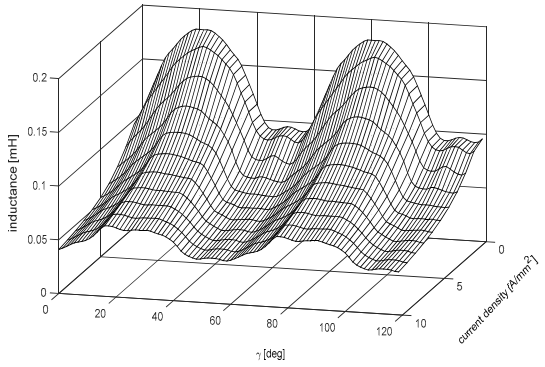

Fig. 10. Self-inductance of the studied six-phase motor.

Using dq-transformations for the modeling of electrical machines provides many advantages. An appropriate dq-transformation converts AC quantities to DC quantities and eliminates the rotor position dependency of the machine's inductances, noticeable in Figure 10 [4].

There are many different approaches reported in the literature addressing the dq-transformation of common three-phase machines. However, the dq-transformation of a six-phase machine differs considerably [5]. The six-phase system can be seen as two 30 deg twisted three-phase systems, which are magnetically coupled. The transformation matrix $\boldsymbol{T}_{\mathrm{dq,2x3}}$ (1), consisting of two common three-phase dq-transformation matrices $\boldsymbol{T}_{\mathrm{dq,3}}$ [7] here denoted with block matrices, transfers the machine's quantities into two dq-systems shifted by 30 deg.

$$\boldsymbol{T}_{\mathrm{dq,23}} = \begin{pmatrix} \boldsymbol{T}_{\mathrm{dq,3}}(\gamma) & \boldsymbol{0}_{3\mathrm{x}3} \\ \boldsymbol{0}_{3\mathrm{x}3} & \boldsymbol{T}_{\mathrm{dq,3}}\left(\gamma - \frac{\pi}{6}\right) \end{pmatrix} \tag{3}$$

Since the transformed dq-inductance matrix obtained by application of $\boldsymbol{T}_{\mathrm{dq,2x3}}$ is not diagonal both dq-systems are still coupled complicating the control of the machine [5]. Finding the eigenvalues and the corresponding eigenvectors allows to conclude a matrix $\boldsymbol{S}$ which diagonalizes the transformed dq-inductance matrix. The overall transformation matrix $\boldsymbol{T}_{\mathrm{dq,6}}$, given in (4), is the matrix multiplication of $\boldsymbol{S}$ and $\boldsymbol{T}_{\mathrm{dq,23}}$ which transforms the machine quantities (current i, voltage u, flux ψ and the machine's parameters, as the inductances L und resistances R) into two decoupled dq-systems.

$$\boldsymbol{T}_{\mathrm{dq,6}} = \frac{2}{6}\cdot\begin{bmatrix} \cos(\gamma) & \cos\left(\gamma-\frac{2\pi}{3}\right) & \cos\left(\gamma-\frac{4\pi}{3}\right) & \cos\left(\gamma-\frac{\pi}{6}\right) & \cos\left(\gamma-\frac{5\pi}{6}\right) & \cos\left(\gamma-\frac{3\pi}{2}\right) \\ -\sin(\gamma) & -\sin\left(\gamma-\frac{2\pi}{3}\right) & -\sin\left(\gamma-\frac{4\pi}{3}\right) & -\sin\left(\gamma-\frac{\pi}{6}\right) & -\sin\left(\gamma-\frac{5\pi}{6}\right) & -\sin\left(\gamma-\frac{3\pi}{2}\right) \\ \frac{1}{2} & \frac{1}{2} & \frac{1}{2} & \frac{1}{2} & \frac{1}{2} & \frac{1}{2} \\ -\cos(\gamma) & -\cos\left(\gamma-\frac{2\pi}{3}\right) & -\cos\left(\gamma-\frac{4\pi}{3}\right) & \cos\left(\gamma-\frac{\pi}{6}\right) & \cos\left(\gamma-\frac{5\pi}{6}\right) & \cos\left(\gamma-\frac{3\pi}{2}\right) \\ \sin(\gamma) & \sin\left(\gamma-\frac{2\pi}{3}\right) & \sin\left(\gamma-\frac{4\pi}{3}\right) & -\sin\left(\gamma-\frac{\pi}{6}\right) & -\sin\left(\gamma-\frac{5\pi}{6}\right) & -\sin\left(\gamma-\frac{3\pi}{2}\right) \\ -\frac{1}{2} & -\frac{1}{2} & -\frac{1}{2} & \frac{1}{2} & \frac{1}{2} & \frac{1}{2} \end{bmatrix} \tag{4}$$

The first and the second row of the transformation matrix create the conventional d- and q-components, respectively, called the d_1- and q_1-components. The fourth and fifth row create additional components in the following denoted as the d_2- and q_2-components. The third and sixth row create two zero sequence components, called the z_1- and z_2-components. As it can be shown, the different pairs of components account for different harmonics in the transformed quantity. So does the d_1- and q_1-system containing the 1st, 11th, 13th ,… harmonics, the d_2- and q_2-system the 5th, 7th ,… harmonics and the z_1- and z_2-system the 3rd, 9th,… harmonics.

The application of the transformation applied to the main voltage equation of a PMSM, the electrical input power can be derived as shown in (5), where ω_{el} is the electric angular frequency.

$$\begin{aligned} P_{\mathrm{el}} &= \vec{i}_{\mathrm{dq}}^{\mathrm{T}} \cdot \vec{u}_{\mathrm{dq}} \\ &= \underbrace{\vec{i}_{\mathrm{dq}}^{\mathrm{T}} \boldsymbol{R}\, \vec{i}_{\mathrm{dq}}}_{\substack{\text{ohmic} \\ \text{losses}}} + \underbrace{\omega_{\mathrm{el}}\, \vec{i}_{\mathrm{dq}}^{\mathrm{T}} \begin{bmatrix} 0 & -1 & 0 & 0 & 0 & 0 \\ 0 & 0 & 0 & 0 & 0 & 0 \\ 1 & 0 & 0 & 0 & 0 & 0 \\ 0 & 0 & 0 & 0 & -1 & 0 \\ 0 & 0 & 0 & 1 & 0 & 0 \\ 0 & 0 & 0 & 0 & 0 & 0 \end{bmatrix} \vec{\psi}_{\mathrm{dq}}}_{\text{mechanical power } P_{\mathrm{mech}}} + \underbrace{\omega_{\mathrm{el}} \vec{i}_{\mathrm{dq}}^{\mathrm{T}} \frac{d}{d\gamma} \vec{\psi}_{\mathrm{dq}}}_{\substack{\text{change of stored} \\ \text{magnetic energy}}} \end{aligned} \tag{5}$$

For the computation of the average torque of a PMSM only the second term is crucial. Hence, the average torque is determined by (6), where ω_{mech} is the mechanical angular frequency and p the number of polepairs.

$$\begin{aligned} T = \frac{P_{\mathrm{mech}}}{\omega_{\mathrm{mech}}} &= p \cdot \begin{pmatrix} i_{\mathrm{d1}} & i_{\mathrm{q1}} & i_{\mathrm{z1}} & i_{\mathrm{d2}} & i_{\mathrm{q2}} & i_{\mathrm{z2}} \end{pmatrix} \begin{pmatrix} -\psi_{\mathrm{q1}} \\ \psi_{\mathrm{d1}} \\ 0 \\ -\psi_{\mathrm{q2}} \\ \psi_{\mathrm{d2}} \\ 0 \end{pmatrix} \\ &= p \cdot \left(\psi_{\mathrm{d1}} i_{\mathrm{q1}} - \psi_{\mathrm{q1}} i_{\mathrm{d1}} + \psi_{\mathrm{d2}} i_{\mathrm{q2}} - \psi_{\mathrm{q2}} i_{\mathrm{d2}}\right) \end{aligned} \tag{6}$$

Considering only the fundamental wave component the d_2- and q_2-components can be neglected, as the fundamental wave is only transformed to the d_1- and q_1-components. This results in a simplified transformation matrix $\boldsymbol{T}_{\mathrm{dq,6}}^{\sim}$, given in (7), as well as a simplified torque computation, given in (8), similar to the common three-phase torque computation [7].

$$\boldsymbol{T}_{\mathrm{dq,6}}^{\sim} = \frac{2}{6}\cdot\begin{bmatrix} \cos(\gamma) & \cos\left(\gamma-\frac{2\pi}{3}\right) & \cos\left(\gamma-\frac{4\pi}{3}\right) & \cos\left(\gamma-\frac{\pi}{6}\right) & \cos\left(\gamma-\frac{5\pi}{6}\right) & \cos\left(\gamma-\frac{3\pi}{2}\right) \\ -\sin(\gamma) & -\sin\left(\gamma-\frac{2\pi}{3}\right) & -\sin\left(\gamma-\frac{4\pi}{3}\right) & -\sin\left(\gamma-\frac{\pi}{6}\right) & -\sin\left(\gamma-\frac{5\pi}{6}\right) & -\sin\left(\gamma-\frac{3\pi}{2}\right) \\ \frac{1}{2} & \frac{1}{2} & \frac{1}{2} & \frac{1}{2} & \frac{1}{2} & \frac{1}{2} \end{bmatrix} \tag{7}$$

$$\begin{aligned} T &= \frac{6}{2} p \cdot \left(\psi_{\mathrm{d1}} i_{\mathrm{q1}} - \psi_{q1} i_{d1}\right) \\ &= \frac{6}{2} p \cdot \left(\left(L_{\mathrm{dd1}} - L_{\mathrm{qq1}}\right) i_{\mathrm{d1}} i_{\mathrm{q1}} + L_{\mathrm{dq1}}\left(i_{\mathrm{q1}}^2 - i_{\mathrm{d1}}^2\right) + \psi_{\mathrm{fd1}} i_{\mathrm{q1}} - \psi_{\mathrm{fq1}} i_{\mathrm{d1}}\right) \end{aligned} \tag{8}$$

The average torque obtained by the described dq-model matches the average torque obtained by the simulation, as it can be seen in Figure 11. For this comparison a unskewed machine model is applied. The average torque of 150 Nm is

achieved with a current density of 9.5 A/mm^2 corresponding to a effective phase-current of 197 A.

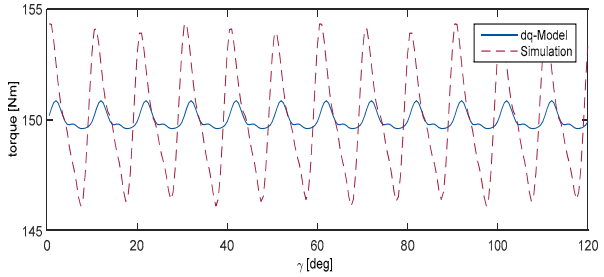

Fig. 11. Comparison of torque obtained by dq-model and simulation.

The torque obtained by the dq-model over the current density is shown in Figure 12. As it is expected, no torque is generated with pure d-current. Furthermore, the maximum torque per ampere curve bends towards a higher j_d/j_q-ratio with increasing torque.

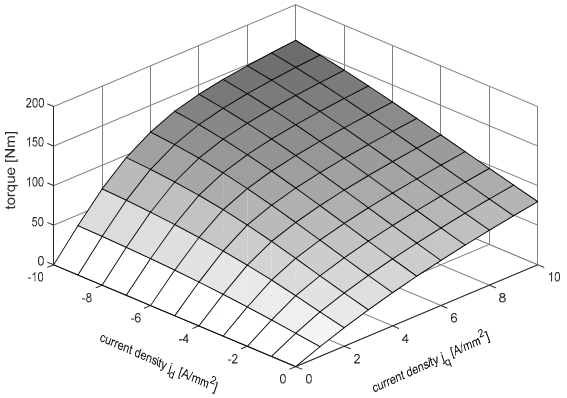

Fig. 12. Torque versus current density j_d and j_q.

The relative error between the torque obtained by the dq-model and the torque obtained by the simulation is plotted in Figure 13. The higher deviation in the region of low q-current is caused by the low torque values. The maximum relative error is below 0.1 %.

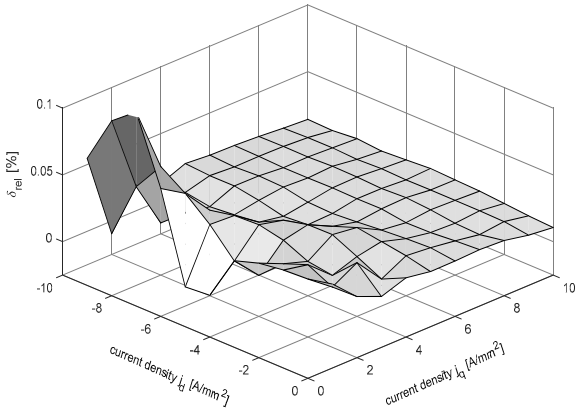

Fig. 13. Relative error of calculated and simulated torque versus current density j_d and j_q.

It is shown that the presented model of the six-phase PMSM describes the machine's operation characteristics and can be used to control and operate the presented machine.

V. Conclusions

The application of a multi-phase VPMSM with six phases, 36 slots three polepairs provides a realistic alternative to the conventionally used three-phase drives. In addition to the avoidance of a large part of the harmonics the motor has a high winding factor of the fundamental wave $\xi_1 = 1$, resulting in a high utilization. With the developed machine model the six-phase machine can be described and operated. The gas cooling designed with high volume flow rates and turbulence is proofed to be a reasonable aperture for unwarming heat in motors core. Its shown that it can be spaced within a hollow rotor. The measurements will be done in the future, followed by a comparison of measurement versus simulation. As a result of R&D work on the project e-MoSys, five patents regarding rotor integrated cooling are filed.

VI. Acknowledgment

The results presented in this paper have been developed in the research project "e-MoSys: Entwicklung und prototypische Umsetzung eines anfordergungsgerechten und modularen Antriebs- und Fahrwerkssystems für ein Elektrofahrzeug" granted by the Ministry of Education and Research (reference number 16N11637).

Federal Ministry
of Education
and Research

References

[1] T. Finken, M. Felden, K. Hameyer, "Comparison and design of different electrical machine types regarding their applicability in hybrid electrical vehicles", *Proc. Conf of International Conference on Electrical Machines*, Vilamoura, Portugal, September 2008, p. 1-5.

[2] Daniel Eggers, Simon Steentjes and Kay Hameyer, "Advanced Iron-Loss Estimation for Nonlinear Material Behavior", *IEEE TRANSACTIONS ON MAGNETICS*, volume 48, number 11, pages 3021-3024, 2012.

[3] Howard W Penrose, Ph.D., Donald Wittmuss, "Evaluation of Vacuum Encapsulation Systems for Integral Motors", *2011 Electrical Insulation Conference*, Annapolis, Maryland, 5 to 8 June 2011.

[4] M. Andriollo, G. Bettanini, G. Martinelli, A. Morini, A. Tortella: Analysis of Double Star Permanent Magnet Synchronous Generators by a General Decoupled d-q Model, *Electric Machines Drives Conference, 2007, IEMDC '07. IEEE International Bd. 1*, 2007, S. 7–12.

[5] Levi, E.; Bojoi, R.; Profumo, F.; Toliyat, H.A.; Williamson, S., "Multiphase induction motor drives - a technology status review," *Electric Power Applications, IET* , vol.1, no.4, pp.489,516, July 2007.

[6] Peng Zhang , Dan M. Ionel and Nabeel A.O. Demerdash, "Saliency Ratio and Power Factor of IPM Motors Optimally Designed for High Efficiency and Low Cost Objectives", *Energy Conversion Congress and Exposition (ECCE), 2014 IEEE*, 14-18 Sept. 2014, Page(s): 3541 - 3547.

[7] T. Herold, D. Franck, E. Lange, K. Hameyer, "Extension of a d-q model of a permanent magnet excited synchronous machine by including saturation, cross-coupling and slotting effects," *Electric Machines & Drives Conference (IEMDC), 2011 IEEE International*, vol., no., pp.1363,1367, 15-18 May 2011.